

# On the convective overstability in protoplanetary discs

Henrik N. Latter<sup>1\*</sup>

<sup>1</sup> DAMTP, University of Cambridge, CMS, Wilberforce Road, Cambridge CB3 0WA, UK

16 August 2018

## ABSTRACT

This paper explores the driving of low-level hydrodynamical activity in protoplanetary-disc dead zones. A small adverse radial entropy gradient, ordinarily stabilised by rotation, excites oscillatory convection (‘convective overstability’) when thermal diffusion, or cooling, is neither too strong nor too weak. I revisit the linear theory of the instability, discuss its prevalence in protoplanetary discs, and show that unstable modes are exact nonlinear solutions in the local Boussinesq limit. Overstable modes cannot grow indefinitely, however, as they are subject to a secondary parametric instability that limits their amplitudes to relatively low levels. If parasites set the saturation level of the ensuing turbulence then the convective overstability is probably too weak to drive significant angular momentum transport or to generate vortices. But I also discuss an alternative, and far more vigorous, saturation route that generates radial ‘layers’ or ‘zonal flows’ (witnessed also in semiconvection). Numerical simulations are required to determine which outcome is favoured in realistic discs, and consequently how important the instability is for disc dynamics.

**Key words:** convection — instabilities — waves — turbulence — protoplanetary discs

## 1 INTRODUCTION

It is increasingly clear from observations that protoplanetary discs are highly structured — exhibiting gaps, asymmetries, and spirals — and thus deviate significantly from simple smooth disc models (Andrews et al. 2011, Muto et al. 2012, Perez et al. 2014, Brogan et al. 2015). Besides these observed features, theory predicts an annular region between roughly 1 AU and 10 AU in which the magnetorotational instability fails to initiate turbulence, but where hydrodynamical processes may hold sway (Gammie 1996, Armitage 2011). Originally termed a ‘dead zone’ (though not nearly so dead as first thought), this region plays a critical role in theories of outburst behaviour and vortex and planet formation (e.g. Armitage et al. 2001, Varnière & Tagger 2006, Kretke et al. 2009, Chatterjee & Tan 2014).

One possible source of hydrodynamical activity is convection. Irradiation from the protostar will certainly generate a negative radial temperature gradient in the disc, though it is unclear if this is sufficient to force the entropy  $S$  to decrease outward as well (a necessary precondition for convection). In fact, observations indicate that on radii  $\gtrsim 20$  AU most disks exhibit  $dS/dR > 0$  and hence convection is impossible (Andrews et al. 2009, 2010; Isella et al. 2009, Guilloteau et al. 2011). The situation is uncertain, however,

at smaller radii, near the disk surface, and around structures such as dead zones, opacity transitions, and gaps; here the sign of the gradient may well be reversed. This paper is relevant to specific disc locations for which this is indeed the case.

The other problem that faces convection is the discs’s strong differential rotation, which would easily negate its negative entropy gradient; according to the Solberg-Høiland criterion, protoplanetary discs are stable. However, certain double-diffusive processes have found ways around this constraint. Examples include: a resistive instability that employs diffusing magnetic fields (Latter et al. 2010a), the subcritical baroclinic instability (SBI, Lesur & Papaloizou 2010), and the convective overstability (Klahr & Hubbard 2014, Lyra 2014), the latter two making use of thermal diffusion (or cooling). It is to the convective overstability that this work is devoted.

Thermal diffusion introduces a crucial time lag between an inertial wave’s dynamical oscillation (an epicycle, essentially) and its associated thermodynamic oscillation. After half an epicycle a fluid blob returns to its starting radius at a different temperature than its surroundings. As a consequence, it suffers a buoyancy acceleration that amplifies the initial oscillation, leading to runaway growth. Such overstable convection was first touched on by Chandrasekhar (1953, 1961) but, as interest originally lay in stellar interiors, researchers focussed on cases in which the oscillations

\* E-mail: hl278@cam.ac.uk

arose not from rotation but from magnetic tension (Cowling 1957) or composition gradients ('semi-convection', Kato 1966). It is only recently, decades later, that oscillatory convection has been raised in the context of accretion discs (Klahr & Hubbard 2014, Lyra 2014), even though it could play an important part in dead zone dynamics. Indeed, the local simulations of Lyra (2014) suggest that the instability's nonlinear saturated state transports a respectable amount of angular momentum and even generates vortices, possibly in conjunction with the SBI.

This paper will revisit both the linear and nonlinear theory of the convective overstability, remaining in the Boussinesq approximation throughout. I reproduce analytic expressions for the growth rate, and show that the fastest growing mode possesses a local growth rate of  $|N^2|/\Omega \sim 10^{-3}\Omega$ , where  $N$  and  $\Omega$  are the radial buoyancy and rotation frequencies of the disc. Its vertical wavelength is short, of order  $\sqrt{\xi/\Omega} \sim 10^{-2}H$  at 1 AU, where  $\xi$  is the thermal diffusivity and  $H$  is the disc scale height, while its radial wavelength is much longer and connects up to the global structure. I also discuss the prevalence of convective overstability in realistic discs, and conclude (in agreement with Lin & Youdin 2015) that it is not widespread, perhaps only appearing in inner disc regions, dead zones, or near gaps. I also show that the unstable modes are nonlinear solutions to the governing equations of Boussinesq hydrodynamics, and thus can grow to arbitrarily large amplitudes, at least in principle. Before a mode grows too powerful, however, it is attacked by parasitic instabilities, the foremost of which involves the well known parametric resonance between inertial waves and an epicycle (e.g. Gammie et al. 2000). Subsequently, an analytical estimate for the overstability's saturation level can be derived that predicts a maximum amplitude of  $|N^2|/\Omega^2$  over the background.

I discuss the nature of the ensuing turbulence, and consider connections with semiconvection, as well as the SBI. In particular, I argue that if the characteristic amplitude of the turbulent state is determined by the parasitic modes and if  $|N| \ll \Omega$ , then its motions will be too axisymmetric and too weak to transport appreciable angular momentum or to generate vortices. If, on the other hand, the saturation culminates in layer formation, as can occur in semiconvection, the turbulent velocities may be orders of magnitude greater and more interesting dynamics may ensue. Numerical simulations are needed to determine which outcome is realistic.

The overstability's turbulent stirring could agitate dust grains, impeding settling but also enhancing the collision frequency and collision speeds of 0.1-1 m particles. Lastly, the convective overstability, being essentially global in radius, may be connected to global dynamics and (more speculatively) excite a small amount of eccentricity, though this cannot be tested in the local model used here.

## 2 MODEL EQUATIONS

Being interested in small scales and subsonic flow, I approximate the protoplanetary disc with the Boussinesq shearing sheet. This model describes a small 'block' of disc centred at a radius  $R_0$  moving on the circular orbit prescribed by  $R_0$  and at an orbital frequency of  $\Omega$ . The block is represented

in Cartesian coordinates with the  $x$  and  $y$  directions corresponding to the radial and azimuthal directions, respectively (see Goldreich & Lynden-Bell 1965).

The governing equations are

$$\partial_t \mathbf{u} + \mathbf{u} \cdot \nabla \mathbf{u} = -\frac{1}{\rho} \nabla P - 2\Omega \mathbf{e}_z \times \mathbf{u} + 2q\Omega x \mathbf{e}_x - N^2 \theta \mathbf{e}_x + \nu \nabla^2 \mathbf{u}, \quad (1)$$

$$\partial_t \theta + \mathbf{u} \cdot \nabla \theta = u_x + \xi \nabla^2 \theta, \quad (2)$$

$$\nabla \cdot \mathbf{u} = 0, \quad (3)$$

where  $\mathbf{u}$  is the fluid velocity,  $P$  is pressure,  $\rho$  is the (constant) background density, and  $\theta$  is the buoyancy variable. The shear parameter of the sheet is denoted by  $q$ , equal to  $3/2$  in a Keplerian disc, and the buoyancy frequency arising from the radial stratification is denoted by  $N$ . Being interested in the optically thicker dead zone, we employ thermal diffusion rather than an optically thin cooling law, as is done in Klahr & Hubbard (2014) and Lyra (2014). Viscosity, denoted by  $\nu$ , has been included for completeness but will be usually set to 0.

Following Lesur & Papaloizou (2010), the stratification length  $\ell$  has been absorbed into  $\theta$ . Thus  $\theta \propto \ell^{-1}(\rho'/\rho)$ , where  $\rho'$  is the perturbation to the background density. The (squared) buoyancy frequency can be determined from

$$N^2 = -\frac{1}{\gamma\rho} \frac{\partial P}{\partial R} \frac{\partial \ln(P\rho^{-\gamma})}{\partial R}, \quad (4)$$

evaluated at  $R = R_0$ . In the above  $\gamma$  is the adiabatic index. Another important quantity is the (squared) epicyclic frequency

$$\kappa^2 = 2(2 - q)\Omega^2. \quad (5)$$

In addition to  $q$ , the system can be specified by two other dimensionless parameters. The Richardson number measures the relative strength of the radial stratification; it is denoted by  $n^2$  and defined via

$$n^2 = -\frac{N^2}{\kappa^2}. \quad (6)$$

In thin astrophysical discs,  $n^2$  is generally small (see Section 3.4). The Prandtl number helps quantify the separation in scales between the thermal lengthscale and the viscous lengthscale; it is denoted by  $\text{Pr}$  and defined via

$$\text{Pr} = \frac{\nu}{\xi}, \quad (7)$$

it too is generally small. Finally, though the outer scale does not appear in the governing equations, it can be useful to define the Peclet number

$$\text{Pe} = \frac{H^2 \kappa}{\xi}, \quad (8)$$

where  $H$  is the vertical scale height. In our problem, this parameter helps quantify the separation in scales between the instability length and the disc thickness.

## 3 LINEAR THEORY

In this section I revisit the analyses presented in Klahr & Hubbard (2014) and Lyra (2014), and provide an analytical

expression for the growth rate in the limit of small Richardson number. I explicate the physical mechanism of instability and apply these results to the conditions expected in protoplanetary discs.

### 3.1 Inviscid eigenproblem

Equations (1)-(3) yield the equilibrium,  $\mathbf{u} = -q\Omega x \mathbf{e}_y$ ,  $\theta = 0$ , and  $P$  a constant. This is perturbed by disturbances proportional to  $e^{st+iKz}$ , where  $s$  is a (complex) growth rate and  $K$  is a (real) vertical wavenumber. We assume that any radial variation exhibited by our modes lie on scales larger than the shearing sheet and does not interfere with its local physics. Viscosity is also dropped, to ease the analysis.

Denoting perturbation with primes, the linearised equations are

$$s u'_x = 2\Omega u'_y - N^2 \theta', \quad (9)$$

$$s u'_y = (q - 2)\Omega u'_x, \quad (10)$$

$$s \theta' = u'_x - \xi k^2 \theta'. \quad (11)$$

Our ansatz ensures that  $u'_z = 0$ , via the incompressibility condition, and  $P' = 0$ , via the  $z$ -component of the momentum equation. The dispersion relation for these modes is easily obtained:

$$s^3 + \beta s^2 + (N^2 + \kappa^2)s + \beta \kappa^2 = 0, \quad (12)$$

where  $\beta = \xi K^2$  is the (length-scale dependent) cooling rate. Apart from differences in notation, Eq. (12) agrees with Eq. (18) in Klahr & Hubbard (2014), Eq. (21) in Lyra (2014), and the inviscid version of Eq. (B2) in Guilet & Müller (2015).

When there is no thermal diffusion whatsoever Eq. (12) is easy to solve and one obtains buoyancy-assisted epicyclic motion. Instability occurs when

$$N^2 + \kappa^2 < 0, \quad (13)$$

i.e. the Solberg-Høiland criterion. When  $\xi$  is nonzero the dispersion relation is a cubic and the analytic solution messy. A numerical solution, using fiducial parameters, is plotted in Fig. 1.

In the natural limit of small Richardson number  $n^2 \ll 1$ , a convenient analytical expression for  $s$  is available, as Guilet & Müller (2015) show. They set  $s = s_0 + s_1 n^2 + \dots$  and to leading order Eq. (12) becomes

$$(s_0^2 + \kappa^2)(s_0 + \beta) = 0,$$

which yields a decaying energy mode and two epicycles. We take one of the epicycles,  $s_0 = i\kappa$ , and at the next order obtain

$$s_1 = -\frac{1}{2} \frac{\kappa^2}{\kappa^2 + \beta^2} (\beta - i\kappa).$$

The real part of the growth rate is hence

$$\text{Re}(s) = -\frac{1}{2} \frac{\beta N^2}{\kappa^2 + \beta^2} + \mathcal{O}(n^4 \kappa), \quad (14)$$

which matches the full solution to Eq. (12) for all  $k$  (or  $\beta$ ) in the appropriate limit. Maximum growth is achieved when  $\beta = \kappa$ , i.e. when  $K = \sqrt{\xi/\kappa}$ , for which

$$\text{Re}(s_{\max}) = -\frac{1}{4} \frac{N^2}{\kappa}, \quad (15)$$

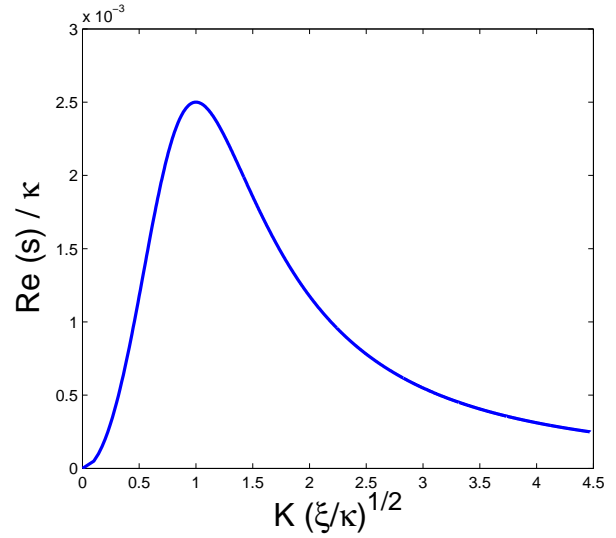


**Figure 1.** Real part of the convective overstability's growth rate as a function of wavenumber  $K$ . The Richardson number is  $n^2 = 0.01$ . The solid line represents the full solution to Eq. (12), but the analytic approximation of Eq. (14) is indistinguishable.

which agrees with Eq. (32) in Lyra (2014).

Three things are noteworthy. First, the Solberg-Høiland criterion no longer determines the onset of instability. Instead, growth occurs when  $N^2 < 0$  (the Schwarzschild criterion); thus the convective overstability has used thermal diffusion to negate the stabilising influence of rotation. Second, the maximum growth rate is independent of the magnitude of thermal diffusion, even though it is crucial to the existence of the instability. Thermal diffusion works as a catalyst of instability, but only fixes its characteristic lengthscale. Third, because its radial wavenumber is zero the mode's group speed  $\partial \text{Im}(s) / \partial K$  is small, proportional to  $n^2$  (and hence much less than the phase speed). As a consequence, there is no risk that the mode energy propagates far away before it grows to appreciable amplitudes.

The eigenfunction of the unstable mode itself consists of a vertical stack of planar fluid sheets each undergoing slowly growing epicycles and each communicating with its neighbours via thermal diffusion. Because vertical motion is absent from the mode, it is relatively impervious to the disc's vertical structure, in particular a stable stratification. Note that if a scale-free cooling law is adopted, rather than thermal diffusion (Klahr & Hubbard 2014, Lyra 2014), the unstable modes can possess an arbitrary dependence on  $z$ . In fact, such a model predicts that *every* scale, from the viscous cut-off all the way to  $H$ , grows at the same maximum rate, a situation that is somewhat artificial and may pose problems when the nonlinear dynamics are simulated.

Putting to one side its vertical dependence, the convective overstability can also be identified as the local manifestation of a global eccentric mode, with azimuthal wavenumber equal to 1 (Ogilvie 2001, Ogilvie & Barker 2014). The convective overstability may thus potentially excite the disc's eccentricity, though this is an idea not pursued in this paper.

Lastly, there also exist modes with non-zero radial

wavenumbers that grow slower and are not treated here (see Lyra 2014). Non-axisymmetric modes, on the other hand, offer only a short period of transient growth before being sheared out, and are also neglected.

### 3.2 Influence of viscosity

In the regime  $n^2 \gg \text{Pr}$ , viscosity only adds a small correction to the maximum growth rate. But it does damp small scales that would be otherwise unstable. In Appendix A, I calculate the critical wavenumber upon which short modes are stabilised. For small Prandtl number it may be estimated by

$$K_c \approx \left(\frac{n^2}{\text{Pr}}\right)^{1/4} K_{\text{fast}}, \quad (16)$$

where  $K_{\text{fast}}$  is the wavenumber of fastest growth. Note that the  $1/4$  power means that the spatial separation between the fastest growing and marginal modes is not as vast as one would first think.

We may also derive a revised stability condition for the convective overstability. When viscosity is present the Schwarzschild criterion is replaced by

$$N^2 < -\frac{2\text{Pr}}{1 + \text{Pr}} \Omega^2. \quad (17)$$

The entropy gradient must be negative *and* sufficiently strong. However, owing to the smallness of  $\text{Pr}$  in real discs, the criterion is only slightly modified. On the other hand, in numerical simulations where  $\nu$  is unrealistically large, Eq. (17) should be kept in mind.

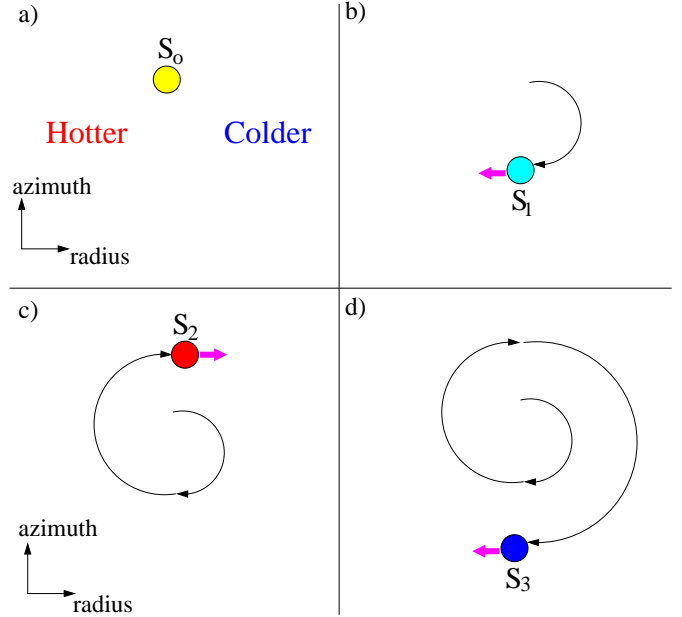
### 3.3 Instability mechanism

Figure 2 illustrates the basic mechanism of the convective instability, drawing on arguments in Cowling (1958). The mechanism is almost identical to that driving the SBI, as described in Lesur & Papaloizou (2010). The only difference is that the convective overstability forces fluid blobs to execute epicycles, while the SBI forces them to circulate around a vortex.

Consider a local patch in the disc-plane exhibiting a weak entropy gradient so that ‘colder’ fluid is at larger radii, and ‘hotter’ fluid is at smaller radii. Suppose a fluid blob at a given radius, associated with an entropy of  $S_0$ , is made to undergo epicyclic motion, panels (a) and (b).

Panel (b) shows the blob after half an epicycle, when it has returned to its original radius. During its outward excursion it has come into contact with colder fluid and has thus exchanged some of its initial heat via thermal diffusion. As a consequence, when it returns to its starting radius it is cooler and possesses a new entropy  $S_1 < S_0$ . Because of this entropy difference the blob suffers an inward buoyancy force (represented by the magenta arrow) that boosts the amplitude of the epicycle.

Panel (c) shows the blob after executing a full epicycle. Again it is back at its starting radius but now it has greater entropy than its surroundings  $S_2 > S_0$  because it has attempted to equilibriate with the hotter fluid at smaller radii. The blob now feels an outwardly directed buoyancy force that further amplifies the epicycle. And panel (d) shows the next phase, where the process runs away.



**Figure 2.** Four panels indicating the convective overstability mechanism. In panel (a) a fluid blob is embedded in a radial entropy gradient. In panel (b) it undergoes half an epicycle and returns to its original radius with a smaller entropy than when it began  $S_1 < S_0$ . It hence feels a buoyancy acceleration inwards and the epicycle is amplified. The process occurs in reverse once the epicycle is complete, shown in panel (c), where now  $S_2 > S_0$ . The oscillations hence grow larger and larger.

Instability would be quenched if thermal diffusion was too efficient or too inefficient. In the first (isothermal) case, at every stage of the epicycle the fluid blob would possess the same entropy as its surroundings. It would hence never feel a buoyancy acceleration. In the second (adiabatic) case, the fluid blob’s entropy would never deviate from  $S_0$  and it would execute buoyancy-adjusted epicycles.

### 3.4 Parameter values and physical scales

#### 3.4.1 Buoyancy frequency and characteristic timescales

I first discuss the sign and magnitude of  $N^2$ . This quantity must be negative for there to be instability, but what do recent observations have to say about this? Let us examine the stability of the disc midplane first. Assuming that  $\gamma = \frac{7}{5}$ , the inviscid instability condition may be re-expressed as  $q_\rho > \frac{5}{2}q_T$ , where  $q_\rho = d \ln \rho / d \ln R$  and  $q_T = d \ln T / d \ln R$  with  $T$  temperature. Taking  $\rho$  at the midplane, this becomes

$$q_\Sigma > \frac{5}{2}q_T + q_H, \quad (18)$$

where  $q_\Sigma = d \ln \Sigma / d \ln R$  and  $q_H = d \ln H / d \ln R$ , and in which  $\Sigma$  is surface density. Equation (18) basically states that instability favours disc radii with fairly flat density profiles, and discs that are less flared. In addition, the stronger the negative temperature gradient the more likely instability, as expected.

To date, the various  $q$  parameters have been estimated from (sub-)mm observations of some two dozen pre-main sequence stars, mainly in the Taurus and Ophiucus star-forming regions (Andrews et al. 2009, Isella et al. 2009, Guil-

loteau et al. 2011). Generally  $q_T$  lies between -0.6 and -0.5 and  $q_H = 1.04 - 1.26$ . There is greater variation in the density structure. Andrews et al. (2009) find that  $q_\Sigma$  can fall between  $-1$  and  $-0.4$ . As a consequence, all but one of the discs in their sample fail to satisfy Eq. (18), with AS 209 perhaps marginally unstable. Isella et al. (2009) and Guilloteau et al. (2011) obtain a larger spread, with  $q_\Sigma$  varying between  $-1.5$  and  $0$  on intermediate to long radii, far from the disk inner edge. Though some inner regions may satisfy Eq. (18), most of the discs in this sample exhibit an insufficiently flat density structure and are hence also generally stable<sup>1</sup>.

The conditions for convective overstability improve, however, the further from the disc midplane. A locally isothermal model with realistic power laws in density and temperature reveals that the magnitude of  $q_\rho$  has decreased by  $\sim 30\%$  at  $z = (3/4)H$ . This is sufficient to push some discs to marginal stability or perhaps better, but a more thorough study of disc structure is necessary to settle the issue. Note that locations higher up in the disc,  $z > (3/4)H$ , are probably inappropriate venues for overstability on account of the magnetorotational turbulence, wind launching, and/or associated planar jets (Fleming & Stone 2003, Bai & Stone 2013, Gressel et al. 2015).

Taking these results on face value, we conclude (as do Lin & Youdin 2015) that most locations in most protoplanetary discs exhibit a positive  $N^2$  and are hence stable to the convective overstability (as well as the SBI). At smaller radii ( $\sim 1$  AU) the picture is less clear because there the disk structure is less well constrained by the observations. This is also true in and around conspicuous disc features such as dead zones (which may be partly shadowed by the disc's hotter inner radii), opacity transitions, and edges, because the fitting models assume smooth disc profiles. These regions could in principle possess unstable entropy gradients, but more advanced numerical modelling is needed to establish whether this is actually the case (see Faure et al. 2014, Flock et al. 2015). Finally, because gas off the midplane possess weaker radial density gradients, instability may also favour locations higher up in the disk. The working hypothesis of this paper is that there are indeed certain disc regions, in particular dead-zones, that are convectively overstable.

Supposing that a disc region is overstable, in order for the instability to have a measurable effect, it must grow sufficiently quickly. The maximum growth rate depends closely on the strength of the magnitude of  $N^2$ , via Eq. (14). But, as discussed above, it is unclear what values it should take. The best we can do is assume that both the pressure and entropy decrease with radius so that  $\partial_R \sim 1/\ell$ . Then

$$N^2 \sim \left(\frac{H}{\ell}\right)^2 \Omega^2, \quad (19)$$

from Eq. (4), where the stratification length  $\ell \lesssim R$  for a smooth gradient (as might be the case deeper in a dead zone), and  $\ell \gtrsim H$  near an abrupt structure (a dead zone

edge or gap edge, for example). Throughout the paper we take a conservative approach and consider  $\ell \sim R$ . With the standard scaling  $H/R \sim 0.05$  we obtain,

$$\text{Re}(s) \sim 10^{-3} \Omega. \quad (20)$$

Thus the e-folding time at 1 AU is roughly 1000 years, plenty of scope for the instability to develop within a protoplanetary disc's lifespan. It should not be forgotten that Eq. (20) may be an underestimate near more abrupt disc structures, for which  $\ell \gtrsim H$ .

### 3.4.2 Prandtl number and characteristic lengthscales

The previous subsection assumes that the fastest growing scales fit into the disc or are not so small that viscosity stabilises them. This needs to be checked. From (14) the dominant vertical scale is  $K \sim \sqrt{\Omega/\xi}$ . A standard expression for the thermal diffusivity at the midplane at 1 AU is

$$\xi = 2.39 \times 10^{12} \left(\frac{\rho}{10^{-9} \text{gcm}^{-3}}\right)^{-2} \left(\frac{T}{100 \text{K}}\right)^3 \times \left(\frac{\kappa_{\text{op}}}{\text{cm}^2 \text{s}^{-1}}\right)^{-1} \text{cm}^2 \text{s}^{-1}, \quad (21)$$

where  $\kappa_{\text{op}}$  is opacity. The reference values are drawn from the minimum mass solar nebula at a few AU (Hayashi et al. 1985) and calculated opacities at low temperatures (Henning & Stognienko 1996). Hence the dominant vertical wavelength at 1 AU is

$$\lambda \sim K^{-1} \sim 10^{10} \text{cm} \sim 0.01 H, \quad (22)$$

which fits comfortably into the disc. It follows that the Peclet number is  $\sim 10^4$ .

The convective overstability exhibits relatively small vertical scales, endorsing the adoption of the local Boussinesq model, yet still far larger than the viscous length. At 1 AU,  $\nu \sim 10^5 \text{cm}^2 \text{s}^{-1}$  and the Prandtl number is  $\sim 10^{-7}$ . On the other hand, the radial scales are unconstrained by the analysis (similarly to magnetorotational channel modes, Balbus & Hawley 1991), and must lie on scales of order  $\ell$  or  $R$ .

## 3.5 Unstable modes are nonlinear solutions

The final important point is that the linear modes explored in this section are also exact nonlinear solutions to the governing equations. Both  $\mathbf{u}$  and  $\theta$  depend on  $z$  and  $t$ , but  $u'_z = 0$ . Therefore all the nonlinear terms in Eqs (1)-(2) vanish:

$$\mathbf{u}' \cdot \nabla \mathbf{u}' = \mathbf{u}' \cdot \nabla \theta' = 0.$$

As a consequence, a convectively overstable mode will grow exponentially even after it leaves the linear regime, and in theory can achieve arbitrarily large amplitudes. A similar property is shared by magnetorotational channel flows (Goodman & Xu 1994).

Of course, the exponential growth cannot continue indefinitely. For a start, the system will ultimately violate the Boussinesq assumptions, i.e. subsonic flow and small thermodynamic variation. It may also be that the mode's global radial structure intervenes to halt the runaway. Perhaps, before either comes into play, parasitic modes, feeding on the

<sup>1</sup> It should be remembered that, because instabilities tend to erase the unstable conditions from which they arise, the observations cannot show disc structures that are 'about to be attacked' by instability but rather structures after the instability has had its way.

mode's strong shear, destroy the mode and initiate a period of hydrodynamical turbulence. It is this last possibility that we explore next.

## 4 PARASITIC INSTABILITIES

### 4.1 Linearised equations

In this section, we view the growing oscillations of Section 3 as part of the basic state and subsequently explore growing perturbations to this state. It is assumed the oscillations have reached an amplitude characterised by the shear rate  $S$ , and though we permit  $S \sim \Omega$  or larger, to ease the calculations the buoyancy frequency is assumed small, so that  $|N| \ll \kappa$ ,  $S$ . Because the parasitic growth rates will be  $\sigma \sim S$ , the buoyancy term may then be dropped from the perturbation equations, and the thermal equation decouples. We may also omit the slow growth of the convectively overstable mode itself, as it is negligible compared to  $\kappa$  and  $S$ . Finally, we set  $q = 3/2$ , and thus  $\kappa = \Omega$ . The equilibrium to leading order may now be written as

$$u_x = S \cos \Omega t \cos Kz, \quad u_y = -\frac{3}{2}\Omega x - \frac{1}{2}S \sin \Omega t \cos Kz,$$

where we have used the eigenvector of Eqs (9)-(10) to describe the oscillatory component of the equilibrium.

Units are chosen so that  $K = 1$ ,  $\kappa = 1$ , and  $\rho = 1$ . The background state is disturbed by velocity and pressure perturbations taking the standard Floquet form,

$$\hat{\mathbf{u}}(t, z)e^{\sigma t + imz + ikx}, \quad \hat{p}(t, z)e^{\sigma t + imz + ikx},$$

where the hatted variables are  $2\pi$ -periodic in both  $t$  and  $z$ . Here  $k$  is a radial wavenumber, and  $\sigma$  and  $m$  are Floquet exponents; the former serves as the growth rate of the perturbation. Note that I neglect non-axisymmetric disturbances; because such modes will be sheared out quickly, they are less effective at killing their hosts. Only at very large  $S$  will they be important.

The linearised equations governing the evolution of these perturbations are

$$\sigma \hat{u}_x = -\partial_t \hat{u}_x - ik \epsilon U \hat{u}_x - \epsilon \partial_z U \hat{u}_z - ik \hat{p} + 2\hat{u}_y, \quad (23)$$

$$\sigma \hat{u}_y = -\partial_t \hat{u}_y - ik \epsilon U \hat{u}_y - \epsilon \partial_z V \hat{u}_z - \frac{1}{2}\hat{u}_y, \quad (24)$$

$$\sigma \hat{u}_z = -\partial_t \hat{u}_z - ik \epsilon U \hat{u}_z - \partial_z \hat{p} - im \hat{p}, \quad (25)$$

$$0 = ik \hat{u}_x + \partial_z \hat{u}_z + im \hat{u}_z, \quad (26)$$

where the background convective oscillation is represented by

$$U = \cos t \cos z, \quad V = -\frac{1}{2} \sin t \cos z, \quad (27)$$

and the parameter  $\epsilon = S/\Omega$  measures the amplitude of the background convective oscillation.

We now have a two-dimensional eigenvalue problem in both  $t$  and  $z$ . The eigenvalue is  $\sigma$ , while the governing parameters are simply  $\epsilon$  and  $k$ . Generally Eqs (23)-(26) must be solved numerically, but in the limits of small and large  $S$  some analytical progress can be made. We treat these asymptotic limits first and then give the numerical solutions.

## 4.2 Asymptotic solutions

### 4.2.1 Large amplitude oscillations

The first limit is perhaps the easiest to understand, though not the most relevant. I assume that the background oscillations are extremely strong, with shear rates  $S \gg \Omega$ . In this regime, parasites grow so fast that the oscillation is destroyed before completing even one cycle. As a consequence, it should be regarded as 'frozen' and, furthermore, the background differential rotation omitted. The problem then reduces to determining the stability of a spatially periodic shear called Kolmogorov flow (Meshalkin & Sinai 1961), an especially well-studied model problem for which numerous results have been proven (see, for example, Beaumont 1981 and Gotoh et al. 1983).

The inflexion point theorem suggests the flow is unstable, and indeed Drazin & Howard (1962) show that instability occurs on  $k < 1$ . A reasonable approximation to the growth rates is derived by Green (1974), who uses a truncated Fourier series to obtain

$$\sigma^2 \approx \frac{k^2(1-k^2)}{2(1+k^2)} \epsilon^2, \quad (28)$$

when  $m = 0$ . Here  $k$  should be understood as the wavenumber in the direction of the shear at any given instant. In agreement with our initial assumption, Eq. (28) yields a growth rate  $\sim S$ .

### 4.2.2 Small amplitude oscillations

Before such large amplitudes are achieved the oscillation will be destroyed by a different class of parasitic mode involving a parametric resonance between the growing epicycle and two inertial waves. The instability is a relation of the famous elliptical instability, which disrupts vortices both in and outside of protoplanetary discs (Pierrehumbert 1986, Bayly 1986, Kerswell 2002, Lesur & Papaloizou 2009, Raiton & Papaloizou 2014). A variant of the instability also attacks accretion discs themselves when the streamlines deviate from non-circular orbits (Goodman 1993), as in the case of eccentric (Papaloizou 2005, Barker & Ogilvie 2014) and warped discs (Gammie et al. 2000, Ogilvie & Latter 2013). Locally this deviation appears as an oscillation with frequency equal to  $\kappa$  and similar in form to the convective overstability mode.

The parametric instability can be understood as a special case of a three-wave coupling (Gammie et al. 2000). The primary overstable oscillation, with frequency  $\kappa$ , provides a means by which two linear inertial waves, of frequencies  $\omega_1$  and  $\omega_2$ , can work together to draw out energy from the primary. In order for this to happen a resonance condition  $\omega_1 + \omega_2 = \kappa$  must be met. Resonance only occurs for a discrete set of  $k$ , each corresponding to a different vertical mode number  $n$ .

Appendix B outlines an asymptotic theory of this resonance in the limit of small oscillation amplitude and for  $m = 0$ . The appropriate regime is  $|N| \ll S \ll \Omega$ : thus the thermal dynamics are omitted, but the rotational dynamics are not. In dimensionless variables the resonance condition is

$$\frac{n}{\sqrt{n^2 + k^2}} + \frac{n+1}{\sqrt{(n+1)^2 + k^2}} = 1, \quad (29)$$

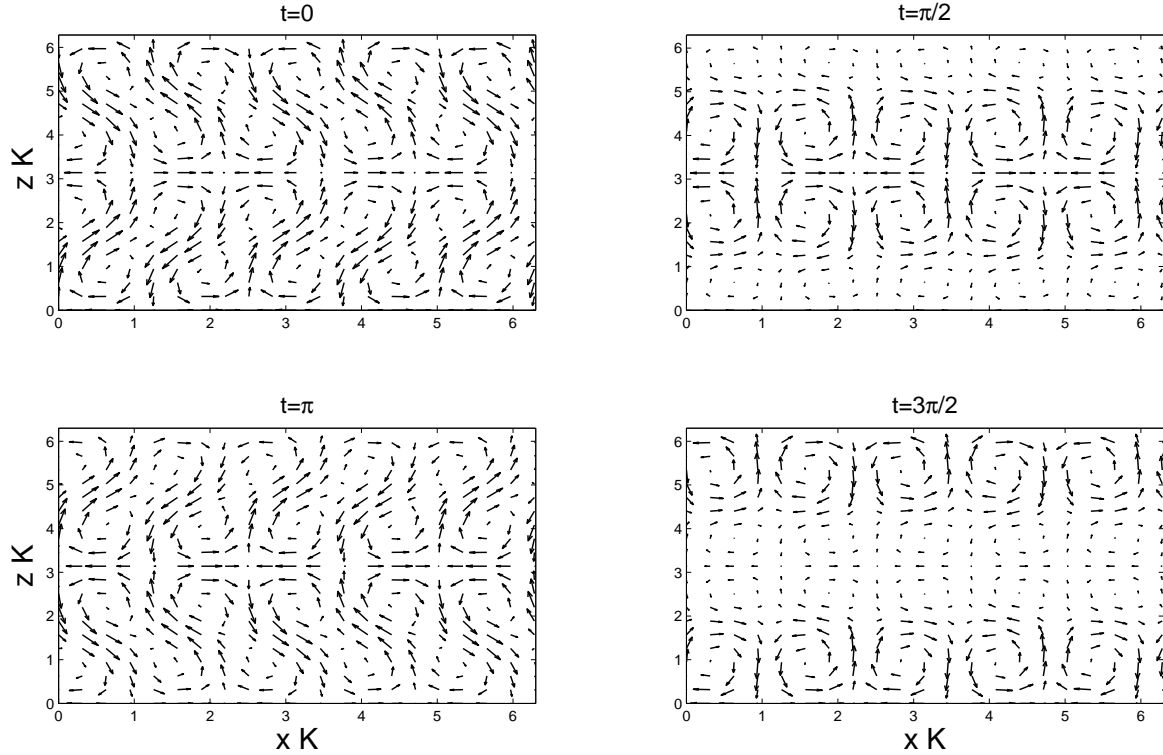


**Figure 4.** Four panels showing the eigenfunction (flows in the  $x$ - $z$  plane) at four different moments during the oscillation. See Section 4.3.

where  $n$  is an integer, describing the vertical wavenumber of the first inertial mode. The first few resonances occur at  $k \approx 2.49, 4.26, 6.02, 7.76, 9.50$ . Note that parametric instability favours much shorter vertical scales than the shear instability of Section 4.2.1. The growth rate to leading order in  $\epsilon$  is given by

$$\sigma^2 = \frac{k^2(1+2\omega_1)^2(\omega_1^2+2\omega_1-n)(\omega_1^2+n)}{64n(1+n)\omega_1(1+\omega_1)} \epsilon^2, \quad (30)$$

where the frequency of the first inertial wave is taken to be

$$\omega_1 = -\frac{n}{\sqrt{n^2+k^2}}. \quad (31)$$

The growth rates corresponding to the first five  $n$  are plotted in Fig. 3a, alongside the full numerical solution. Finally, as  $n \rightarrow \infty$  the growth rates plateau to a constant maximum value, given by  $\sigma \approx \frac{3\sqrt{3}}{32} \epsilon$ .

### 4.3 Numerical solutions

In this section Eqs (23)-(26) are solved numerically using a pseudo-spectral technique. I partition the  $2\pi$ -periodic  $t$  and  $z$  domains into  $M_t$  and  $M_z$  cells and represent each dependent variable as a vector of length  $M_t M_z$ . Derivatives are described using appropriate matrices (Boyd 2002), upon which (23)-(26) may be approximated by a  $4M_t M_z \times 4M_t M_z$  algebraic eigenvalue problem, the eigenvalues of which are the growth rates  $\sigma$ . These are obtained by the QZ algorithm

or an Arnoldi method (Golub & van Loan 1996). For moderate  $k$ ,  $M_t = M_z = 30$  yields converged growth rates.

The real part of the growth rate  $\sigma$  is plotted in Fig. 3 as a function of radial wavenumber  $k$ . Two illustrative values of the oscillation amplitude are chosen,  $\epsilon = 0.1$  and  $\epsilon = 1$ . The vertical wavenumber of the mode's envelope  $m$  is set to zero. The top panel lies in the small amplitude regime, and hence I also plot the growth rates produced by the asymptotic theory of Section 4.2.2, as blue diamonds. Instability occurs in distinct bands located at the resonant  $k$  values predicted by Eq. (29). The asymptotic growth rates are in good agreement with the numerical results, which validates both the analytic theory and the computations. As is typically the case, the larger the  $k$  the wider each resonant band, and at some large value the bands overlap and the instability becomes more complicated in nature than the simple three-wave resonance idea. This is also true the larger  $\epsilon$ , as is clear from the bottom panel of Fig. 3. Here  $\epsilon = 1$  and instability occurs for all  $k$  above a critical value. As expected, the growth rates are an order of magnitude greater than the  $\epsilon = 0.1$  case.

In Fig. 4 a representative eigenmode is shown, when  $\epsilon = 0.1$  and  $k = 2.486$ . The figure comprises four snapshots in the  $x$ - $z$  plane of the velocity taken at equally spaced moments during its  $2\pi$  cycle. The mode comes from the first band of parametric instability in Fig. 3a, and consists of  $n = 1$  and  $n = 2$  inertial waves coupled via the overstable oscillation. Note its characteristic oblique motions: the ra-

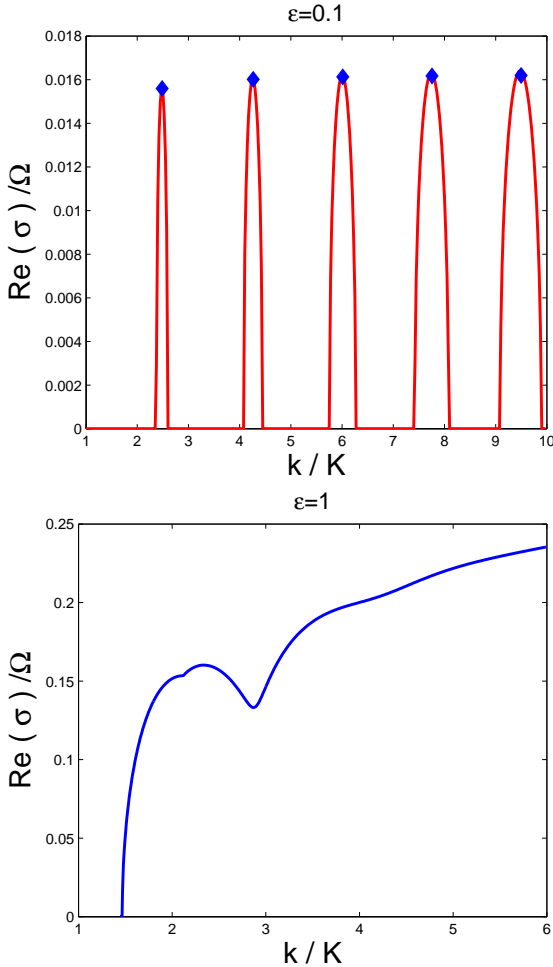


**Figure 3.** Parasitic growth rates  $\sigma$  as a function of radial wavenumber  $k$  for two different amplitudes. The top panel is for  $\epsilon = 0.1$ , the bottom for  $\epsilon = 1$ . In the top panel the predictions of the asymptotic theory are represented by blue diamonds.

dial and vertical mode speeds are most closely correlated in panels 1 and 3 ( $t = 0, \pi$ ), when the background radial shear take its largest values (cf. Eq. (27)). The associated Reynolds stresses of the mode are thus able to extract the overstability’s energy. Similar behaviour is observed in the instability of a warp (Ogilvie & Latter 2013).

#### 4.4 Maximum amplitude

It is possible to estimate a maximum saturation amplitude of the convective overstability by comparing the growth of the overstability itself with that of its parasites. Similar calculations have been carried out in the magnetorotational channel context (Pessah & Goodman 2009, Latter et al. 2010b), but the overstability problem is made easier by the axisymmetry of the parasitic modes. They cannot be sheared away by the differential rotation.

In the previous subsections, the slow growth of the oscillation was neglected and so  $\epsilon$  was taken to be a constant. In this section its time dependence is reinstated, so that (in dimensionless variables)  $\epsilon = \epsilon_0 e^{st}$ , where  $\epsilon_0$  is the os-

cillation’s starting amplitude (the level of the background fluctuations), and  $s \sim n^2$  is its growth rate.

A crude estimate for the time it takes a parasitic mode to overrun its host may be derived by equating the growth rates of parasite and host,  $s \sim \sigma$  (Pessah & Goodman 2009). The oscillation’s amplitude at this point is then easy to calculate:  $\epsilon_{\max} \sim n^2$ . Returning to dimensional units, the maximum shear is

$$S_{\max} \sim \frac{|N^2|}{\Omega}. \quad (32)$$

Given the smallness of  $N^2$  in protoplanetary discs, this is not a large value at all, only some  $10^{-3}$  the background shear rate (cf. Section 3.4). In realistic discs, the convective overstability grows so slowly that it is overrun by parasitic modes before it extracts appreciable energy from the thermal gradient.

This rough estimate may be improved upon by setting the *amplitudes* of the oscillation and parasite to be equal, rather than the growth rates. The parasitic mode’s amplitude we denote by  $p$ , and its growth is determined from the ODE  $dp/dt = \sigma(t)p$ , where  $\sigma \sim \epsilon$ . This equation yields  $p \sim p_0 \exp[(\exp(st) - 1)\epsilon_0/s]$ , where  $p_0$  is the initial amplitude of the parasite. Setting  $\epsilon = p$  produces a nonlinear equation for the time of destruction, which may be solved in terms of special functions. The maximum oscillation amplitude may then be computed:

$$\epsilon_{\max} \sim -n^2 W_{-1} \left( -\frac{p_0}{n^2} e^{-\epsilon_0/n^2} \right), \quad (33)$$

where  $W_{-1}$  is the second real branch of the Lambert W-function (Corless et al. 1996). Note that the final amplitude depends not only on  $n^2$  but also on the initial conditions. If next we assume that both the overstability and the parasite grow simultaneously from the same reservoir of small amplitude noise ( $< n^2$ ), then we have the asymptotic estimate

$$\epsilon_{\max} \sim n^2 \ln \left( \frac{n^2}{\epsilon_0} \right). \quad (34)$$

This shows that the dependence on the initial condition is weak and that (32) is largely unaltered: convective oscillations are destroyed at low amplitudes.

## 5 NONLINEAR SATURATION

### 5.1 Parasitic theory

Once an isolated overstable mode is overrun by a parasite the flow breaks down into a disordered state. Let us suppose that the nonlinear dynamics that follow are controlled by the emergence and decline of these fastest growing overstable modes. How might this dynamical situation work? One possibility is that the system settles on a weakly nonlinear state, with the three resonant waves joined by a small number of shorter wavelength modes. These shorter modes, ordinarily stabilised by viscosity, will remove the energy input by the instability and let the system reach a statistically steady state. The nonlinear standing waves observed in some semiconvection simulations may be an example of this (Mirouh et al. 2012). Though likely in simulations (with their relatively large Pr), real discs may struggle, however, to host such low-order nonlinear dynamics. Another possibility is that the emergence and destruction of overstable

modes could control developed turbulence in which many more modes participate. Pessah & Goodman (2009) make such an argument to explain the level of magnetorotational turbulence in shearing boxes, but being axisymmetric the parasites considered here are much more effective because they do not shear out (see also Latter et al. 2010b). Whatever its details, a parasitic theory of saturation would then argue that Eq. (32) sets not only the maximum amplitude of a single overstable oscillation but also the saturation amplitude of the ensuing turbulence.

Equation (32) predicts that the convective overstability generates only a very mild level of turbulence in realistic discs. Because the typical strain rate is usually much less than  $\Omega$ , the flow will be essentially axisymmetric. And if one estimates the typical turbulent lengthscale by  $1/K$ , then associated velocities will be gentle:

$$v_{\text{turb}} \sim 10^{-2} n^2 c_s \quad (35)$$

at 1 AU, where  $c_s$  is the local sound speed (cf. Section 3.2). Because of its low amplitude and axisymmetry, the saturated state should not drive significant angular momentum transport nor generate vortices via SBI (or another mechanism). The appearance of both phenomena in the simulations of Lyra (2014) can be attributed to a strong stratification,  $n^2 \sim 0.1$ , which may occur only in special regions of the disc, perhaps near very abrupt disc features.

## 5.2 Connections with semiconvection

Of course, the parasitic theory of saturation may only be part of the story. While it should reliably predict the initial amplitude of the turbulent flow, on longer times the turbulence could evolve according to other dynamics altogether. The saturation of semi-convection is illuminating in this respect, as it shares many of the features of convective overstability in discs. (Indeed, in two dimensions the mathematical formalisms are almost identical.) Instead of relying on angular momentum and entropy gradients, semiconvection emerges in the presence of composition and entropy gradients (Kato 1966, Rosenblum et al. 2011). Its nonlinear development takes one of two courses: (a) mild turbulent convection or (b) large-scale ‘layering’ of convective zones over strongly stratified interfaces (Turner 1968, Merryfield 1995). The turbulent transport in the second course is far greater than in the first by at least an order of magnitude, but it only arises when the background stratification is sufficiently strong (Rosenblum et al. 2011, Mirouh et al. 2012). In fact, there exists a critical buoyancy frequency  $|N_c^2|$ , below which the turbulence is weak and above which it suddenly becomes much more intense. This critical value depends closely on  $\text{Pr}$  (Mirouh et al. 2012).

Can the convective overstability in discs exhibit similar bimodal behaviour? In the disc context the layers would be combined zonal and elevator flows, and thus would correspond to rings of concentrated vorticity. Indeed, the 2D simulations of Lyra (2014) develop large-scale radial structure at late times that could be identified as a ‘semi-convective layer’. Key questions are: what is the critical value of  $N^2$  below which radial layers fail to develop (if such a value exists)? Which side of this value do realistic dead zones fall? What about other more abrupt disc features? Obviously if layers dominate the overstability’s long term saturation then

the ‘parasitic theory’ must be discarded, and the convective overstability may instigate more vigorous, and interesting, dynamics. Simulations are currently underway to test these competing ideas.

Zonal flows may be susceptible to the Kelvin-Helmholtz instability, shedding vortices as they degenerate. Lyra’s 3D simulations also manifest vortices, though it is unclear if they arise from the breakdown of zonal layers or by the SBI, seeded by vigorous non-axisymmetric turbulence. Again it is important to note that these simulations are strongly stratified, with  $n^2 \approx 0.1$ . More realistic values may yield a less vigorous and more axisymmetric state, one that may struggle to seed vortices directly. Again this needs to be checked in dedicated 3D simulations.

## 6 DISCUSSION

Ordinarily the angular momentum gradient in a protoplanetary disc is sufficiently strong to stabilise a negative entropy gradient, if one exists. But because thermal diffusion is far more efficient than viscous diffusion, double diffusive instabilities arise that can unleash the energy stored in the adverse gradient. These include the subcritical baroclinic instability and the convective overstability (Lesur & Papaloizou 2010, Klahr & Hubbard 2014, Lyra 2014). The resistive instability, on the other hand, uses magnetic fields to diffuse angular momentum faster than heat and is hence double-diffusive in the opposite sense (Latter et al. 2010a). These various mechanisms may liven up the dead zones of protoplanetary discs, though it is unclear if any one of them is the answer to the question of angular momentum transport.

In this paper I revisit the linear and nonlinear dynamics of the convective overstability. Because the linear modes are also nonlinear solutions, my focus has been on the parasitic modes that limit their amplitude, the idea being that the parasites control the saturation level of the ensuing turbulent dynamics. This approach predicts that the overstability generates only very weak turbulence, with a strain field  $\sim |N^2|/\Omega \sim 10^{-3}\Omega$ . The conclusion is that the flow remains axisymmetric and rather gentle, unable to transport much angular momentum nor generate vortices. However, near very abrupt disc structures, such as edges,  $|N^2|$  may be larger and greater activity might be anticipated. But I also explore alternative ideas, drawing on recent work in semi-convection that shows when  $|N^2|$  crosses a critical value the flow splits into thermo-compositional layers that greatly enhance transport (Rosenblum et al. 2011, Mirouh et al. 2012). Something similar may occur in simulations of the overstability, the layers taking the form of ‘zonal flows’ (Lyra 2014). Future work should establish the critical  $|N^2|$  above which this takes place, and whether we expect this behaviour in realistic discs.

If convective overstability is present, which is not always assured, what is its role in the disc dynamics? One possible application is to the excitation of random motions in disc solids, thereby influencing their collision speeds and frequencies. The greatest effect will be on marginally coupled particles, whose stopping time is similar to the typical turbulent turnover time ( $\sim 1/\Omega$  for inertial wave turbulence). These particles should have radii of roughly 10 cm to 1 m (Chiang & Youdin 2010). The velocity dispersion induced by

the coupling will be of order  $v_{\text{turb}}$ , a fairly mild enhancement in most cases. The turbulent flow may also concentrate such particles, further amplifying collision rates, though this can only be checked by detailed numerical simulations (Hogan & Cuzzi 2007, Pan & Padoan 2013).

In conclusion, the significance of the overstability, vis-à-vis other hydrodynamical processes, essentially comes down to the magnitude of  $N^2$ . It sets the base level of turbulent motions (cf. Eq. (35)) and whether the system selects a gentle or more vigorous state (cf. Section 5.2). Thus further constraints on protoplanetary disc structure and further numerical simulations are needed to help properly assess the instability's place in disc dynamics.

## ACKNOWLEDGMENTS

I thank the reviewer, Steve Balbus, for a helpful set of comments that improved the manuscript. I also thank Gordon Ogilvie, Sebastien Fromang, Geoffroy Lesur, Andrew Youdin, and John Papaloizou for helpful tips and suggestions. I am also grateful to Hubert Klahr and Wlad Lyra for clarifying some of their work and for inspiring me to have a look at the problem. Finally I am indebted to Jerome Guilet who generously read through an earlier version of the manuscript and who suggested valuable improvements to Section 4.4 particularly. This research is partially funded by STFC grant ST/L000636/1.

## REFERENCES

- Armitage, P. J., 2011. *ARAA*, 49, 195.  
 Armitage, P. J., Livio, M., Pringle, J. E., 2001. *MNRAS*, 324, 705.  
 Andrews, S. M., Wilner, D. J., Hughes, A. M., Chunhua, Qi, Dullemond, C. P., 2009. *ApJ*, 659, 705.  
 Andrews, S. M., Wilner, D. J., Espaillat, C., Hughes, A. M., Dullemond, C. P., McClure, M. K., Qim C., Brown, J. M., 2011. *ApJ*, 732, 42.  
 Balbus, S. A., Hawley J. F., 1991. *ApJ*, 376, 214.  
 Barker, A. J., Ogilvie, G. I., 2014. *MNRAS*, 445, 2637.  
 Bai, X., Stone, J. M., 2013. *ApJ*, 769, 76.  
 Bayly, B. J., 1986. *PRL*, 57, 2160.  
 Beaumont, D. N., 1981. *JFM*, 108, 461.  
 Boyd, J. P., 2001. *Chebyshev and Fourier Spectral Methods*, 2nd edn. Dover Press, New York.  
 Brogan, C. L. and 84 coauthors, 2015. *ApJL* accepted.  
 Chandrasekhar, S., 1953. *RSPSA*, 217, 306.  
 Chandrasekhar, S., 1961. *Hydrodynamic and hydromagnetic stability*, Clarendon, Oxford.  
 Chiang, E., Youdin, A. N., 2010. *AREPS*, 38, 493.  
 Corless, R. M., Gonnet, G. H., Hare, D. E. G., Jeffrey, D. J., Knuth, D. E., 1996. *Adv. Comp. Math.*, 5, 329.  
 Cowling, T. G., 1957. *Magnetohydrodynamics*, Interscience Publishers, New York.  
 Drazin, P. G., Howard, L. N., 1962. *JFM*, 14, 257.  
 Faure, J., Fromang, S., Latter, H., 2014. *AA*, 564, 22.  
 Fleming, T., Stone, J. M., 2003. *ApJ*, 585, 908.  
 Flock, M., Ruge, J. P., Dzyurkevich, N., Henning, Th., Klahr, H., Wolf, S., 2015. *AA*, 574, 68.  
 Gammie, C. F., 1996. *ApJ*, 457, 355.  
 Gammie, C. F., Goodman, J., Ogilvie, G. I., 2000. *MNRAS*, 318, 1005.  
 Goldreich, P., Lynden-Bell, D., 1965. *MNRAS*, 130, 125.

- Golub, G. H., van Loan, C. F., 1996. *Matrix Computations*. Johns Hopkins Univ. Press, Baltimore.  
 Goodman, J., 1993. *ApJ*, 406, 596.  
 Goodman, J., Xu, G., 1994. *ApJ*, 432, 213.  
 Gotoh, K., Yamada, M., Mizushima, J., 1983. *JFM*, 127, 45.  
 Guilloteau, S., Dutrey, A., Pié tu, V., Boehler, Y., 2011. *AA*, 529, 105.  
 Green, J. S. A., 1974. *JFM*, 62, 273.  
 Gressel, O., Turner, N. J., Nelson, R. P., McNally, C. P., 2015. *ApJ*, 801, 84.  
 Guilet, J., Müller, E., 2015. *MNRAS*, 450, 2153.  
 Hayashi, C., Nakazawa, K., Nakagawa, Y., 1985. *Protostars and Planets II*. University of Arizona Press, Tucson, AZ, p. 1100.  
 Henning, T., Stognienko, R., 1996. *AA*, 311, 291.  
 Hogan, R. C., Cuzzi, J. N., 2007. *PhRvE*, 75, 6305.  
 Isella, A., Carpenter, J. M., Sargent, A. I., 2009. *ApJ*, 701, 1746.  
 Kato, S., 1966. *PASJ*, 18, 367.  
 Kerswell, R. R., 2002. *AnRFM*, 34, 83.  
 Klahr, H., Hubbard, A., 2014. *ApJ*, 788, 21.  
 Kretke, K. A., Lin, D. N. C., Garaud, P., Turner, N., J., 2009. *ApJ*, 690, 407.  
 Latter, H. N., Bonart, J. F., Balbus, S., A., 2010a. *MNRAS*, 405, 1831.  
 Latter, H. N., Fromang, S., Gressel, O., 2010b. *MNRAS*, 406, 848.  
 Lesur, G., Papaloizou, J. C. B., 2009. *AA* 498, 1.  
 Lesur, G., Papaloizou, J. C. B., 2010. *AA*, 513, 60.  
 Lyra, W., 2014. *ApJ*, 789, 77.  
 Merryfield, W. J., 1995. *ApJ*, 444, 318.  
 Meshalkin, L. D., Sinai, Ia., G., 1961. *JAMM*, 25, 1700.  
 Mirouh G. M., Garaud, P., Stellmach, S., Traxler, A. L., Wood, T. S., 2012. *ApJ*, 750, 61.  
 Muto, T., and 61 coauthors, 2012. *ApJ*, 748, 22.  
 Ogilvie, G. I., Latter, H. N., 2013. *MNRAS*, 433, 242.  
 Pan, L., Padoan, P., 2013. *ApJ*, 776, 12.  
 Papaloizou, J. C. B., 2005. *AA*, 432, 743.  
 Perez, L. M., Isella, A., Carpenter, J. M., Chandler, C. J., 2014. *ApJ*, 783, 13.  
 Pessah, M. E., Goodman, J., 2009. *ApJ*, 698, 72.  
 Pierrehumbert, R. T., 1986. *PRL*, 57, 2157.  
 Raiton, A. D., Papaloizou J. C. B., 2014. *MNRAS*, 445, 4409.  
 Rosenblum, E., Garaud, P., Traxler, A., Stellmach, S., 2011. *ApJ*, 731, 66.  
 Turner, J. S., 1968. *JFM*, 33, 183.  
 Varniere, P., Tagger, M., 2006. *AA*, 446, 13.  
 Youdin, A. N., Goodman, J., 2005. *ApJ*, 620, 459.

## APPENDIX A: VISCOUS LINEAR THEORY

If viscosity is introduced into the linearised equations of (9)-(11) one can derive the following dispersion relation

$$s^3 + a_2 s^2 + a_1 s + a_0 = 0, \quad (\text{A1})$$

where

$$\begin{aligned} a_2 &= K^2 \xi + 2K^2 \nu, \\ a_1 &= K^4 \nu^2 + 2K^4 \xi \nu + \kappa^2 + N^2, \\ a_0 &= K^2 \xi (K^4 \nu^2 + \kappa^2) + K^2 \nu N^2, \end{aligned}$$

(see also Guilet & Müller 2015).

In the regime  $n^2 \gg \text{Pr}$  the viscosity only adds an order  $\text{Pr}$  correction to the maximum growth rate. On smaller scales its effects are more severe and it will ultimately stabilise the modes. I first derive the critical  $K$  when this occurs. As this corresponds to a Hopf bifurcation,  $s = i\omega$  at criticality, in which  $\omega$  is a real frequency. On substituting

this into the dispersion relation, one obtains the two equations

$$-\omega^3 + a_1\omega = 0, \quad -a_2\omega^2 + a_0 = 0,$$

which, after some manipulation, yield an expression for the critical wavenumber

$$K_c^4 = -\frac{2\text{Pr} - n^2(1 + \text{Pr})}{2\text{Pr}(1 + \text{Pr})^2} \frac{\xi^2}{\kappa^2}. \quad (\text{A2})$$

For small Pr, we have the useful estimate

$$K_c \approx \left(\frac{n^2}{\text{Pr}}\right)^{1/4} K_{\text{fast}}, \quad (\text{A3})$$

where  $K_{\text{fast}} \approx \sqrt{\xi/\kappa}$  is the wavenumber of the fastest growing mode. Note in particular the quartic root. Though both Pr and  $n^2$  are small, the viscous cutoff need not be so well separated from  $K_{\text{fast}}$ . If  $n^2 \sim 10^{-3}$  and  $\text{Pr} \sim 10^{-7}$  then  $K_c \sim 10K_{\text{fast}}$ . The unusual quartic expression comes about because the viscous frequency  $\sim \nu K^2$  and the growth rate at small  $K$  is  $\sim -N^2/(\xi K^2)$ , from Eq. (14). Equating the two frequencies gives rise to that fourth power.

In an inviscid gas all scales are unstable when  $N^2 < 0$ . Viscosity, however, alters this condition. It kills off the instability everywhere whenever the numerator in (A2) is negative. This yields the following instability criterion

$$N^2 < -\frac{2\text{Pr}}{1 + \text{Pr}} \Omega^2, \quad (\text{A4})$$

which replaces that of Schwarzschild. Thus the entropy gradient must be both negative *and* sufficiently strong. According to Section 3.4, the right side of (A4) is  $\sim 10^{-7}$ , and so in practice only exceptionally weak negative gradients are stabilised. In fact, we need to also consider the outer scale:  $K_c > 1/H$  or else the instability will not fit into the disc. The instability criterion then picks up another small correction term, and becomes

$$N^2 < -\frac{2\text{Pr}}{1 + \text{Pr}} \Omega^2 - \frac{2\text{Pr}(1 + \text{Pr})}{\text{Pe}^2}. \quad (\text{A5})$$

## APPENDIX B: PARAMETRIC INSTABILITY

In this section I solve the system (23)-(26) to leading order in the small oscillation amplitude,  $\epsilon$ . From the start I set  $m = 0$ , to make life simple.

The followings expansions are assumed:  $\sigma = \epsilon\sigma_1 + \dots$ , and

$$\begin{aligned} \hat{u}_x &= u_0 + \epsilon u_1 + \dots, & \hat{u}_y &= v_0 + \epsilon v_1 + \dots, \\ \hat{u}_z &= w_0 + \epsilon w_1 + \dots, & \hat{p} &= p_0 + \epsilon p_1 + \dots \end{aligned}$$

These are thrown into the linearised equations and the various orders in  $\epsilon$  collected. At leading order the convective oscillation does not appear, and the four equations can be combined into  $\mathcal{L}p_0 = 0$ , where

$$\mathcal{L} = (\partial_t^2 + 1)\partial_z^2 - k^2\partial_t^2. \quad (\text{B1})$$

This equation has solutions  $p_0 \propto E_n \equiv e^{inz - i\omega t}$  for vertical wavenumber  $n$  and frequency  $\omega$ . Because the solutions must be  $2\pi$ -periodic in  $z$ , the wavenumber  $n$  takes integer values. For such solutions to exist, however, the following solvability condition must hold,

$$\omega^2 = \frac{n^2}{k^2 + n^2}, \quad (\text{B2})$$

which is, of course, the dispersion relation for inertial waves in accretion discs. The general solution at this order is an infinite sum (over  $n$ ) of the individual inertial waves. However we are only interested in neighbouring modes that can come into resonance with the background oscillation. These are the  $n$  and  $n + 1$  modes, with associated frequencies  $\omega_1$  and  $\omega_2$ , calculated from Eq. (B2). For resonance to occur  $\omega_1 + \omega_2 = 1$ , which yields the condition Eq. (29), in the main text. Thus

$$p_0 = AE_n + BE_{n+1}, \quad (\text{B3})$$

where  $A$  and  $B$  are constants. Without loss of generality, we set  $B = 1$ . Finally, the velocity components follow from

$$u_0 = -\frac{n^2}{\omega k} p_0, \quad v_0 = \frac{n^2 i}{2k\omega^2} p_0, \quad w_0 = \frac{n}{\omega} p_0. \quad (\text{B4})$$

At the next order, we obtain  $\mathcal{L}p_1 = f$ , where the right hand side is

$$f = (\partial_t^2 a + 2\partial_t b)ik + (\partial_t^2 + 1)\partial_z c, \quad (\text{B5})$$

and

$$\begin{aligned} a &= \sigma u_0 + ikU u_0 + \partial_z U w_0, \\ b &= \sigma v_0 + ikU v_0 + \partial_z V w_0, \\ c &= \sigma w_0 + ikU w_0. \end{aligned}$$

Solvability of this equation requires that  $f$  possesses no term proportional to the solution of the homogeneous problem. Multiplying  $f$  by  $E_n^*$  and integrating over  $t$  and  $z$ , then doing the same with  $E_{n+1}^*$ , gives two solvability conditions, essentially equations for  $A$  and  $\sigma$ . After some tedious algebra, we obtain the growth rate, as a function of  $n$ , which is Eq. (30) in the main text.

At large  $n$ , the resonance condition is satisfied when

$$k^2 = 3n^2 + 3n + \mathcal{O}(1),$$

which correspond to a frequency  $\omega_1 = -\frac{1}{2} + \frac{3}{16}n^{-1} + \mathcal{O}(n^{-2})$ . Putting these expressions into (30) gives, to leading order,  $\sigma_1 = \frac{3\sqrt{3}}{32}$ .